AMERICAN SOCIETY FOR MICROBIOLOGY | Applied and Environmental Microbiology®

GEOMICROBIOLOGY

Metabolic Performance and Fate of Electrons during Nitrate-Reducing Fe(II) Oxidation by the Autotrophic Enrichment Culture KS Grown at Different Initial Fe/N Ratios

Jianrong Huang,[a,b] Adrian Mellage,[c,d] Julian Pavon Garcia,[d] David Glöckler,[e] Susanne Mahler,[e] Martin Elsner,[e] Natalia Jakus,[a,f] Muammar Mansor,[a] Hongchen Jiang,[b] Andreas Kappler[a,g]

[a]Geomicrobiology, Department of Geoscience, University of Tuebingen, Tuebingen, Germany
[b]State Key Laboratory of Biogeology and Environmental Geology, China University of Geosciences, Wuhan, China
[c]Hydrogeology, Civil and Environmental Engineering, University of Kassel, Kassel, Germany
[d]Hydrogeology, Department of Geosciences, University of Tuebingen, Tuebingen, Germany
[e]Analytical Chemistry and Water Chemistry, Technical University of Munich, Munich, Germany
[f]School of Architecture, Civil and Environmental Engineering, École Polytechnique Fédérale de Lausanne, Lausanne, Switzerland
[g]Cluster of Excellence, EXC 2124, Controlling Microbes to Fight Infection, Tuebingen, Germany

ABSTRACT Autotrophic nitrate-reducing Fe(II)-oxidizing (NRFeOx) microorganisms fix CO_2 and oxidize Fe(II) coupled to denitrification, influencing carbon, iron, and nitrogen cycles in pH-neutral, anoxic environments. However, the distribution of electrons from Fe(II) oxidation to either biomass production (CO_2 fixation) or energy generation (nitrate reduction) in autotrophic NRFeOx microorganisms has not been quantified. We therefore cultivated the autotrophic NRFeOx culture KS at different initial Fe/N ratios, followed geochemical parameters, identified minerals, analyzed N isotopes, and applied numerical modeling. We found that at all initial Fe/N ratios, the ratios of $Fe(II)_{oxidized}$ to $nitrate_{reduced}$ were slightly higher (5.11 to 5.94 at Fe/N ratios of 10:1 and 10:0.5) or lower (4.27 to 4.59 at Fe/N ratios of 10:4, 10:2, 5:2, and 5:1) than the theoretical ratio for 100% Fe(II) oxidation being coupled to nitrate reduction (5:1). The main N denitrification product was N_2O (71.88 to 96.29% at Fe/^{15}N ratios of 10:4 and 5:1; 43.13 to 66.26% at an Fe/^{15}N ratio of 10:1), implying that denitrification during NRFeOx was incomplete in culture KS. Based on the reaction model, on average 12% of electrons from Fe(II) oxidation were used for CO_2 fixation while 88% of electrons were used for reduction of NO_3^- to N_2O at Fe/N ratios of 10:4, 10:2, 5:2, and 5:1. With 10 mM Fe(II) (and 4, 2, 1, or 0.5 mM nitrate), most cells were closely associated with and partially encrusted by the Fe(III) (oxyhydr)oxide minerals, whereas at 5 mM Fe(II), most cells were free of cell surface mineral precipitates. The genus *Gallionella* (>80%) dominated culture KS regardless of the initial Fe/N ratios. Our results showed that Fe/N ratios play a key role in regulating N_2O emissions, for distributing electrons between nitrate reduction and CO_2 fixation, and for the degree of cell-mineral interactions in the autotrophic NRFeOx culture KS.

IMPORTANCE Autotrophic NRFeOx microorganisms that oxidize Fe(II), reduce nitrate, and produce biomass play a key role in carbon, iron, and nitrogen cycles in pH-neutral, anoxic environments. Electrons from Fe(II) oxidation are used for the reduction of both carbon dioxide and nitrate. However, the question is how many electrons go into biomass production versus energy generation during autotrophic growth. Here, we demonstrated that in the autotrophic NRFeOx culture KS cultivated at Fe/N ratios of 10:4, 10:2, 5:2, and 5:1, ca. 12% of electrons went into biomass formation, while 88% of electrons were used for reduction of NO_3^- to N_2O. Isotope analysis also showed that denitrification during NRFeOx was incomplete in culture KS and the main N denitrification product was N_2O. Therefore, most electrons stemming from Fe(II) oxidation seemed to be used

Editor John R. Spear, Colorado School of Mines

Address correspondence to Andreas Kappler, andreas.kappler@uni-tuebingen.de.
The authors declare no conflict of interest.

Received 7 February 2023
Accepted 11 February 2023

for N_2O formation in culture KS. This is environmentally important for the greenhouse gas budget.

KEYWORDS nitrate reduction, Fe(II) oxidation, culture KS, Fe/N ratio, electron balance, geomicrobiology, iron biogeochemistry

Microbially mediated nitrate-reducing Fe(II) oxidation (NRFO) was first described by Straub et al. (1) more than 2 decades ago. In pH-neutral and anoxic environments, nitrate-reducing Fe(II)-oxidizing (NRFeOx) microorganisms are able to oxidize Fe(II) coupled to complete or incomplete denitrification. Thus, they play vital roles in Fe-N interactions, iron redox transformation, nitrate removal, and the formation of the greenhouse gas N_2O (2–5). Evidence suggests that these microorganisms are ubiquitous in nature, having been found in various types of environments, such as ditches and brackish water lagoons (1), freshwater lakes (6, 7), marine coastal sediment (8), groundwater (9), submarine hydrothermal systems (10), wetlands (11), sludges (12), and paddy field soils (13). NRFeOx microorganisms can be classified into three different types according to the interaction between nitrate-reducing bacteria and Fe(II) oxidation (3). The first class, autotrophic NRFeOx, use Fe (II) as the electron donor for CO_2 fixation (biomass production) and nitrate reduction (energy generation) without amendment of organic carbon, such as enrichment culture KS (named after the scientist that isolated it, Kristina Straub) (1, 14). The second class, mixotrophic NRFeOx microbes such as *Acidovorax* sp. strain BoFeN1 (15, 16), require an organic substrate (e.g., acetate or lactate) in addition to Fe(II) as a cosubstrate. The third class, heterotrophic denitrifying bacteria (chemodenitrifiers) catalyze Fe(II) oxidation as a result of the abiotic reaction of Fe(II) with reactive N intermediates (e.g., NO_2^- and NO), by-products of heterotrophic denitrification. An example of the heterotrophic class is the hypersaline enrichment culture FeN-CKL (17). The proposed reaction mechanism of NRFO is shown in equation 1.

$$10Fe^{2+} + 2NO_3^- + 24H_2O \rightarrow 10Fe(OH)_3 + N_2 + 18H^+ \quad (1)$$

According to the reaction above, a theoretical stoichiometric ferrous iron-to-nitrogen (Fe/N) ratio of 5:1 is required for the complete reduction of NO_3^- to N_2 gas (1). For autotrophic NRFeOx, the theoretical stoichiometric Fe/N mass ratio should be even greater than 5, if the electrons needed for CO_2 fixation are also considered (8). For autotrophic NRFO, it has been proposed that electrons stemming from Fe(II) oxidation go through the electron transfer chain for energy generation and are ultimately accepted by carbon dioxide and nitrate (18, 19). However, the question of which fraction of electrons stemming from Fe(II) oxidation go either into biomass production (CO_2 fixation) or energy generation (nitrate reduction) during autotrophic growth remains, which is of great importance for the understanding the microbial physiology of this metabolic type of microorganisms.

Denitrification consists of several reduction reactions in which NO_3^- is sequentially transformed to NO_2^-, NO, N_2O, and finally N_2 gas (20, 21). While the final (desired) product, N_2, is an inert gas, local conditions and microbial functional potential can lead to the accumulation of undesirable reactive intermediates during denitrification. Incomplete denitrification can pose an added threat to the natural environment, degrading cells themselves, and human health (22). For example, NO_2^- can cause methemoglobinemia and respiratory infections in humans (23); the accumulation of NO_2^- and NO has a toxic effect on cells (24–27), while the accumulation of N_2O yields potent greenhouse gas release into the atmosphere (28, 29). Several studies reported the accumulation of reactive intermediates during NRFO, in particular NO_2^- and N_2O (30–33). For instance, one previous study demonstrated that 41% of NO_3^- was reduced to N_2O as the final denitrification product by the autotrophic NRFeOx enrichment culture AG (Altingen Groundwater) (9). In the presence of other microorganisms, the accumulated intermediate N compounds can be further reduced, yielding complete denitrification in the presence of sufficient electron donors and microbial functional potential. Moreover, reductive intermediate (e.g., NO_2^- and N_2O)

accumulation during NRFO was suggested to be related to Fe/N ratios (34, 35). Nitrous oxide emissions were promoted at high Fe/N ratios (4:1 to 10:1) by the mixotrophic NRFeOx bacterium *Paracoccus denitrificans* (22). The latter suggests that the Fe/N ratios may play a critical role in regulating N_2 and N_2O emissions and nitrate removal during NRFO and their subsequent undesirable environmental impacts (12). However, the metabolic performance and community dynamics at different initial Fe/N ratios as well as the denitrification products of autotrophic NRFeOx (for instance, for the enrichment culture KS) remain unclear. A better understanding of the functional potential of known NRFeOx bacteria that reduce nitrate in the environment is required to better predict the secondary risks associated with reactive intermediate accumulation (22).

Culture KS is a robust chemolithoautotrophic nitrate-reducing Fe(II)-oxidizing enrichment culture that stems from samples collected from a ditch in Bremen, Germany, in the mid-1990s (1). It has been cultivated autotrophically and continuously over more than 2 decades in two different laboratories at the University of Tuebingen, Germany (culture KS-Tueb), and the University of Wisconsin—Madison, USA (culture KS-Mad) (18, 36). Under autotrophic conditions, these cultures perform Fe(II) oxidation coupled to nitrate reduction immediately after inoculation and slows down after 3 days (36). It was reported that culture KS was capable of nearly complete oxidation of uncomplexed Fe(II) with the reduction of nitrate to N_2 (1). The dominant strain in culture KS is the designated Fe(II) oxidizer belonging to the family *Gallionellaceae*, with a flanking community including several heterotrophic organisms (e.g., *Bradyrhizobium*, *Rhodanobacter*, *Nocardioides*, and *Thiobacillus*) (14, 18, 19). Furthermore, the detailed composition, in particular of the heterotrophic flanking communities, is dependent on the laboratory in which the culture KS was cultivated, as the two are slightly different (KS-Tueb versus KS-Mad) (18). The relative sequence abundance of *Gallionellaceae* in culture KS differs from 96% in culture KS-Tueb to 42% in culture KS-Mad, apparently as a result of different inoculum concentrations (1% in KS-Tueb, as was used in the present study, versus 10% in KS-Mad) (3). Over time, culture KS has sustained a stable microbial consortium and appeared reproducible, with only slight fluctuations in the microbial consortium composition among the different transfers under autotrophic growth conditions (19). Based on the above-mentioned traits, the enrichment culture KS offers a robust model microbial consortium to study autotrophic nitrate reduction coupled to Fe(II) oxidation in an (aquatic) environment (19, 36).

In this study, we investigated the metabolic performance and electron partitioning of the autotrophic NRFeOx culture KS, cultivated at different initial molar Fe/N ratios (10:4, 10:2, 10:1, 5:2, 5:1, and 10:0.5). By coupling monitoring of geochemical species, cell growth, mineral identity, cell-mineral associations, reaction modeling, and nitrogen isotope fractionation, we aimed to quantify the degree of denitrification (in)completeness, shed light on the autotrophic reaction and cell growth processes, and quantify the electron balance between CO_2 fixation (biomass production) and nitrate reduction (energy generation). Our study provides a quantitative interpretation of the relative distribution of electrons to biomass production versus energy generation in the autotrophic NRFeOx culture KS grown at different initial Fe/N ratios.

RESULTS

Kinetics of nitrate-reducing Fe(II) oxidation by the autotrophic culture KS at different initial Fe/N ratios. The measured and simulated temporal evolution of Fe(II) oxidation and nitrate reduction in the autotrophic culture KS at different initial Fe/N ratios is shown in Fig. 1 and in Fig. S1 in the supplemental material. In all biotic treatments, the oxidation of Fe(II) coupled to nitrate reduction was evident after 24 h of incubation and slowed down to stop at or shortly after 96 h. Even though both Fe(II) and NO_3^- were still present after 96 h, we did not observe any further denitrification. The latter was captured by our model by considering a nonbioavailable fraction of Fe (II) (37). Our reaction model was able to accurately capture the extent of Fe(II) oxidation, nitrate reduction, and biomass production for the simulated Fe/N ratios (10:4, 10:2, 5:2, and 5:1). In addition, our model captured the measured accumulation of N_2O, with a slight systematic overestimation for the 10:4 and 10:2 ratios. At the end of the

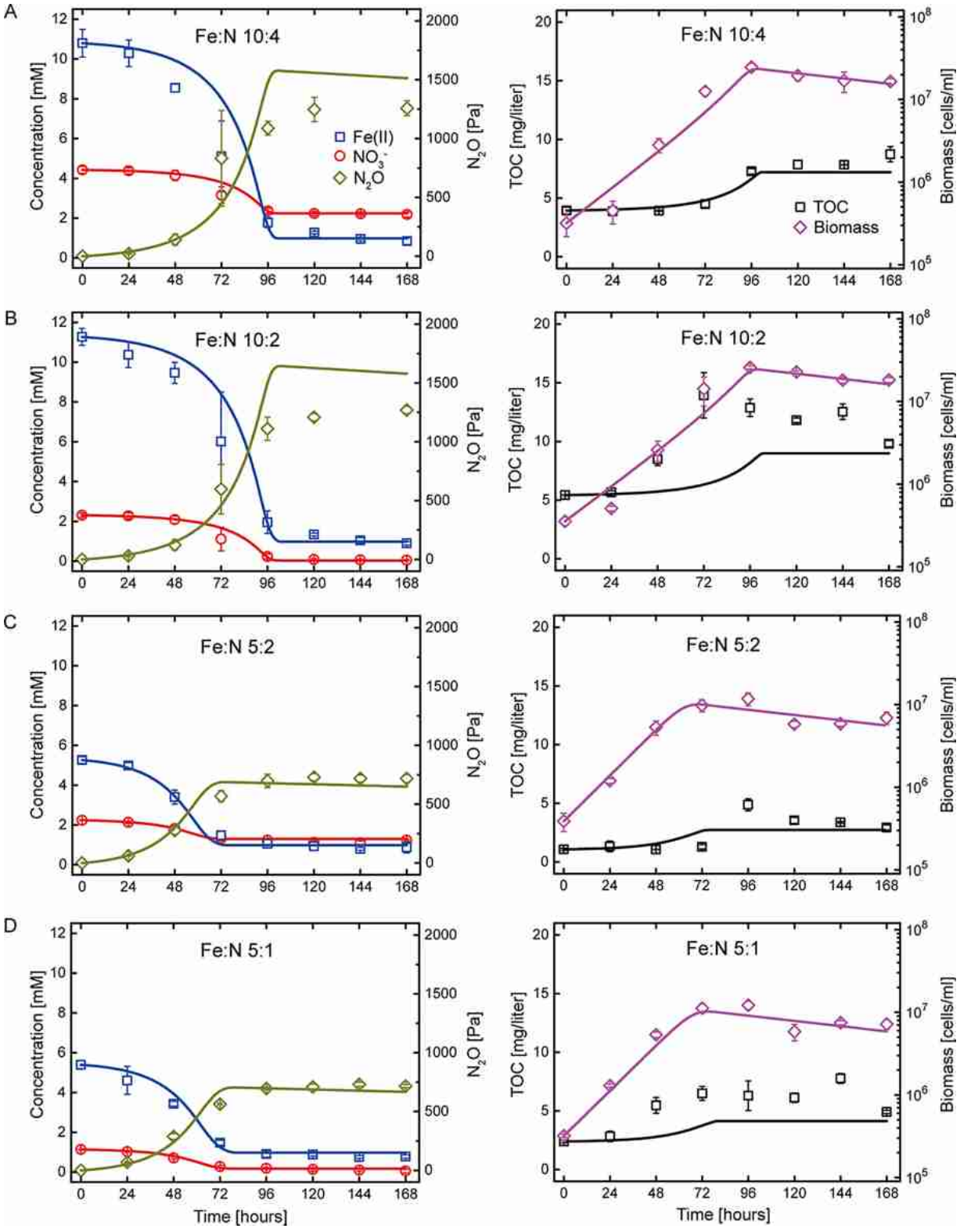

FIG 1 Simulation (lines) and experimental data (symbols) showing Fe(II), nitrate, N_2O gas, TOC, and biomass concentrations for the autotrophic NRFeOx culture KS cultivated at four initial Fe/N ratios (10:4 [A], 10:2 [B], 5:2 [C], and 5:1 [D]). Error bars represent standard deviations of the means (n = 3).

TABLE 1 Concentrations of Fe(II) oxidized, nitrate reduced (at 168 h), and average experimental ratios at six different initial Fe/N ratios

Initial Fe/N ratio	Sample ID	Concn (mM) of:		Stoichiometry of $Fe(II)_{oxidized}/nitrate_{reduced}$	Avg exptl ratio	Theoretical ratio[a]
		Fe(II) oxidized	Nitrate reduced			
10:4	KS1	9.70	2.10	4.61	4.44 ± 0.35	5:1
	KS2	10.68	2.29	4.67		
	KS3	9.43	2.34	4.03		
10:2	KS4	10.70	2.36	4.52	4.59 ± 0.06	5:1
	KS5	10.38	2.25	4.62		
	KS6	10.03	2.17	4.62		
10:1	KS7	5.11	1.16	4.42	5.11 ± 0.61	5:1
	KS8	5.85	1.05	5.57		
	KS9	5.94	1.11	5.35		
5:2	KS10	4.72	1.04	4.55	4.37 ± 0.16	5:1
	KS11	4.36	1.02	4.29		
	KS12	4.40	1.03	4.26		
5:1	KS13	4.27	1.00	4.28	4.27 ± 0.06	5:1
	KS14	4.71	1.12	4.20		
	KS15	4.85	1.12	4.32		
10:0.5	KS16	2.84	0.53	5.39	5.94 ± 0.78	5:1
	KS17	3.07	0.55	5.60		
	KS18	3.70	0.54	6.84		

[a]Complete denitrification.

incubation, the maximum amount of N_2O produced was observed at Fe/N ratios of 10:4 and 10:2, respectively, while a lower production of N_2O was detected at Fe/N ratios of 10:1, 5:2, and 5:1. For comparison, the N_2O production at a Fe/N ratio of 10:0.5 was about 0.6 times that observed at Fe/N ratios of 10:1, 5:2, and 5:1 (Fig. S2). No N_2O was detected in all abiotic controls. Despite minor discrepancies, we were able to calibrate a single set of parameters to describe all experimental scenarios (Table S1).

The extent of electron acceptor and donor consumption, however, varied depending on the initial Fe/N ratios (Table 1). Averages of 9.94 mM and 10.37 mM Fe(II) were oxidized and 2.24 mM and 2.26 mM nitrate were reduced within 168 h at Fe/N ratios of 10:4 and 10:2, respectively. At an Fe/N ratio of 10:1, culture KS consumed on average 5.63 mM Fe(II) and 1.11 mM nitrate. When cultured at Fe/N ratios of 5:2 and 5:1 culture KS consumed an average of 4.49 mM and 4.61 mM Fe(II) and reduced 1.03 mM and 1.08 mM nitrate, respectively. Culture KS cultivated at a Fe/N ratio of 10:0.5 consumed on average 3.21 mM Fe(II) and 0.54 mM nitrate. No further reduction of nitrate was observed once Fe(II) oxidation stopped and vice versa (Fig. S1). At all initial Fe/N ratios, the experimental ratios of oxidized Fe(II) to reduced nitrate were slightly higher (at Fe/N ratios of 10:1 and 10:0.5) or lower (at Fe/N ratios of 10:4, 10:2, 5:2, and 5:1) than the theoretical stoichiometry for 100% Fe(II) oxidation being coupled to nitrate reduction (5:1) (Table 1). Ferrous iron was not oxidized and nitrate was not reduced in the presence of heat-inactivated cells (30 min at 80°C) in abiotic controls (Fig. S1). Furthermore, we did not measure accumulation of NO_2^- and/or NH_4^+ during any of the incubations (Fig. S3). In the biotic treatments and abiotic controls at different initial Fe/N ratios, no obvious changes in total Fe [Fe(tot)] concentrations were observed during the experiments (Fig. S3A and D).

Concurrent with electron donor and acceptor consumption, cell density and total organic carbon (TOC) concentrations increased in all reactors, although no organic carbon was amended in any setup. The accumulation of TOC was offset in time, relative to the increase in cell density (Fig. 1), which motivated the formulation of separate cell division (affecting cell numbers) and biomass synthesis (affecting organic carbon) reaction rates in our model. (Note that the temporal offset between the increase in cells

and that of TOC varied between experiments and was particularly evident for the 10:4 and 5:2 ratios, ranging on the order of 10 to 20 h.) In all cases, maximum (measured) cell densities—1.62×10^7, 1.79×10^7, 9.67×10^6, 6.51×10^6, 6.86×10^6, and 4.00×10^6 cells/mL at Fe/N ratios of 10:4, 10:2, 10:1, 5:2, 5:1, and 10:0.5, respectively (Fig. S4A and C)—coincided with the drop in Fe(II) concentrations to the nonbioavailable amount and dropped in the absence of denitrification. The delayed TOC concentration increase, relative to increasing cell counts, yielded average accumulations of 4.79, 4.38, 3.26, 1.85, 2.51, and 1.96 mg/L for Fe/N ratios of 10:4, 10:2, 10:1, 5:2, 5:1, and 10:0.5, respectively (Fig. S4B and D). No changes in cell numbers and TOC contents were observed in the abiotic controls (Fig. S4).

Morphology and identity of minerals formed by the NRFeOx culture KS cultivated at different Fe/N ratios. At the end of the incubation, the color of the precipitates present in the incubation bottles was brownish or yellowish in the microbially active setups at Fe/N ratios of 10:4, 10:2, 10:1, and 10:0.5, while a greenish color was observed in culture KS cultivated at Fe/N ratios of 5:2 and 5:1 (Fig. S5). In abiotic controls, the color of the precipitates remained whitish-gray, which was the same as that observed in the original medium after the addition of ferrous iron [likely due to Fe(II) phosphate or Fe(II) carbonate precipitation].

As a consequence of Fe(II) oxidation, secondary minerals were formed in culture KS. However, the Fe/N ratios influenced the interactions and associations of cells with the newly formed Fe(III) minerals. Scanning electron microscopy (SEM) images showed that most cells were closely associated with and partially encrusted by the Fe(III) precipitates at Fe/N ratios of 10:4, 10:2, 10:1, and 10:0.5, whereas fewer cells were associated with and encrusted by Fe(III) minerals at Fe/N ratios of 5:2 and 5:1 (Fig. 2). Furthermore, structural fibrils, possibly an extracellular polymeric substance (EPS), were potentially excreted by the cells when cultivated at Fe/N ratios of 5:2 and 5:1, and these fibrils were closely associated with minerals formed during Fe(II) oxidation (Fig. S6). X-ray diffraction (XRD) patterns showed that the dominant Fe(III) precipitates produced by the autotrophic NRFeOx culture KS were poorly crystalline at all Fe/N ratios (Fig. S7). The energy dispersive X-ray analysis (EDX) spectra collected from the surfaces of the biogenic iron oxidation products mainly revealed the presence of C, O, Fe, Na, Al, Si, P, and K (Fig. S8). The high proportion of Si and O is caused by the background of the glass slides used to fix the samples for analysis, while Na and K are likely residues from the culture medium.

Community composition of the autotrophic NRFeOx culture KS cultivated at different initial Fe/N ratios. Six separate clone libraries were established from KS cultures grown at the different initial Fe/N ratios (Fig. S9). Three different operational taxonomic units (OTUs; 97% 16S rRNA gene similarity cutoff) were distinguished in the clone libraries. All clone libraries were dominated by OTU 1 (*Gallionella* sp., 96.17 to 97.79% similarity), which accounts for more than 80% relative 16S rRNA gene sequence abundance at all Fe/N ratios. OTU 1 also showed 96.25% and 96.08% similarity to the iron-oxidizing bacteria *Ferriphaselus* sp. and *Sideroxydans* sp., respectively. In addition to the designated Fe(II) oxidizer *Gallionella* sp., less abundant heterotrophic organisms, such as *Rhodanobacter denitrificans* (OTU 2) at Fe/N 10:2 and 10:0.5, *Bradyrhizobium liaoningense* (OTU 3) at Fe/N 5:1 were also detected (Fig. S9). OTU 2 and OTU 3 were 95.36 to 99.49% and 99.45% similar to *Rhodanobacter denitrificans* and *Bradyrhizobium liaoningense*, respectively.

Quantification of N_2O and N_2 using N isotope-labeled nitrate. In our setups amended with $^{15}NO_3^-$, on average, 9.83, 5.24, and 5.44 mM Fe(II) were oxidized and 2.10, 1.11 and 1.09 mM $^{15}NO_3^-$ were reduced at Fe/^{15}N ratios of 10:4, 5:1, and 10:1 (Fig. S10), yielding ratios of $Fe(II)_{oxidized}$ to $nitrate_{reduced}$ of 4.37 to 4.97 (Table S2). At the end of the incubation, the amount of $^{15}N_2O$ produced was consistent with unlabeled groups (Fig. 3). Geochemical analyses and ^{15}N isotope results showed that the main denitrification product was $^{15}N_2O$ at the end of the experiment, which accounted for 72.55 to 95.83%, 71.88 to 96.29%, and 43.13 to 66.26% of the reduced NO_3^- at Fe/^{15}N ratios of 10:4, 5:1, and 10:1, respectively (Fig. S11). No nitrate reduction to $^{15}N_2$ was reliably detected in culture KS at these three initial Fe/^{15}N ratios (Fig. 3). The values of the

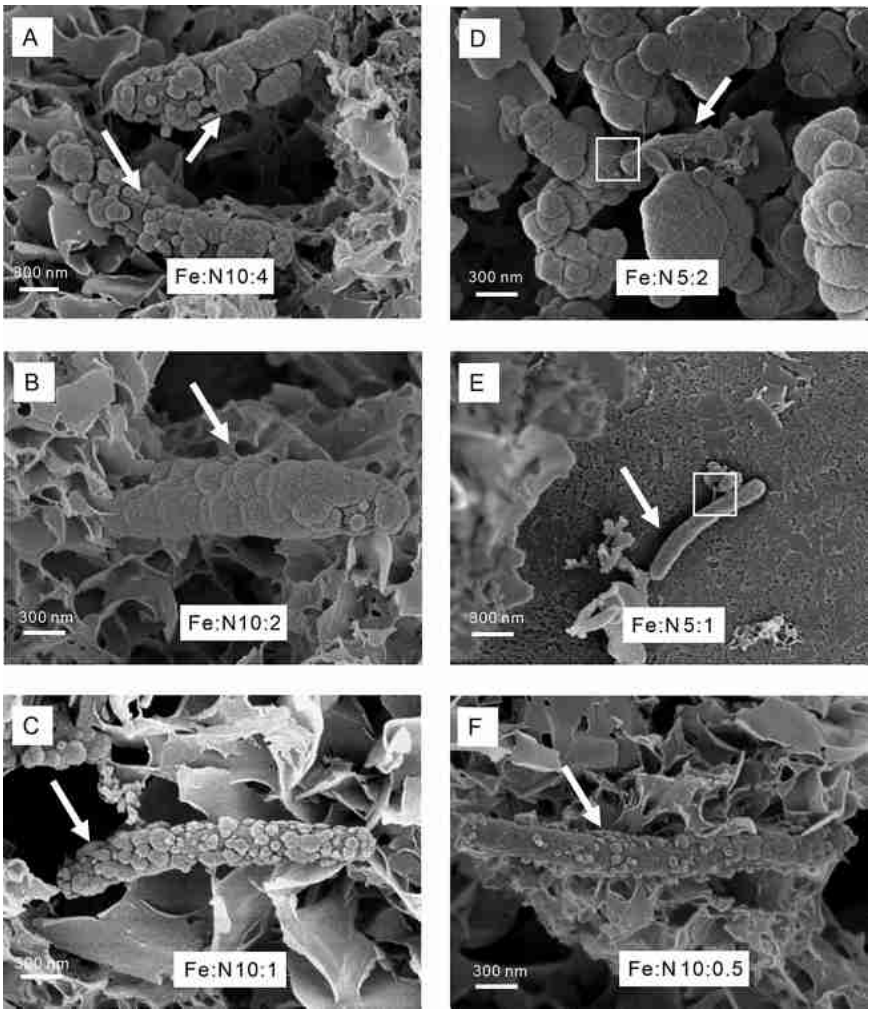

FIG 2 Scanning electron micrographs of cells in the autotrophic NRFeOx culture KS cultivated at different initial Fe/N ratios after 96 h of cultivation. Arrows indicate cells; boxes indicate structural fibrils which were potentially excreted by the cells.

unlabeled NO_3^- controls (at hours 0, 72, and 168) showed good agreement with the corresponding biotic and labeled samples (Fig. 3). No $^{15}N_2O$ or $^{15}N_2$ production was detected in any of the abiotic controls (at hours 0, 72, and 168).

DISCUSSION

Initial Fe(II)/NO_3^- ratios impact the physiology of autotrophic NRFeOx culture KS. The absolute concentration of Fe(II) and/or the initial ratio of electron donor [Fe(II)] versus electron acceptor (nitrate) (initial Fe/N ratio) are expected to regulate the metabolic performance of the nitrate-reducing Fe(II) oxidation process by the autotrophic culture KS. Our results showed that indeed, the values of oxidized Fe(II), reduced nitrate, and cell growth varied in culture KS cultivated at six different initial Fe/N ratios (Fig. 1 and Fig. S1). The experimental ratios of oxidized Fe(II) to reduced nitrate in all treatments were slightly higher (average, 5.11 to 5.94 at Fe/N ratios of 10:1 and 10:0.5) or lower (average, 4.27 to 4.59 at Fe/N ratios of 10:4, 10:2, 5:2, and 5:1) than the theoretical stoichiometry for 100% Fe(II) oxidation being coupled to nitrate reduction (5:1), but the ratio was still close to this 5:1 ratio (Table 1). In a previous study, similar ratios of oxidized Fe(II) to reduced nitrate were reported in culture KS, where the authors measured ratios of 4.25 to 4.8 when 10 mM Fe(II) and 4 mM nitrate were added initially (19, 36). In fact, the theoretical stoichiometry should be greater than 5 in autotrophic NRFeOx microorganisms, because the electrons stemming from Fe(II) oxidation are, in addition to nitrate reduction, also used for biomass production (CO_2 fixation) (8, 14).

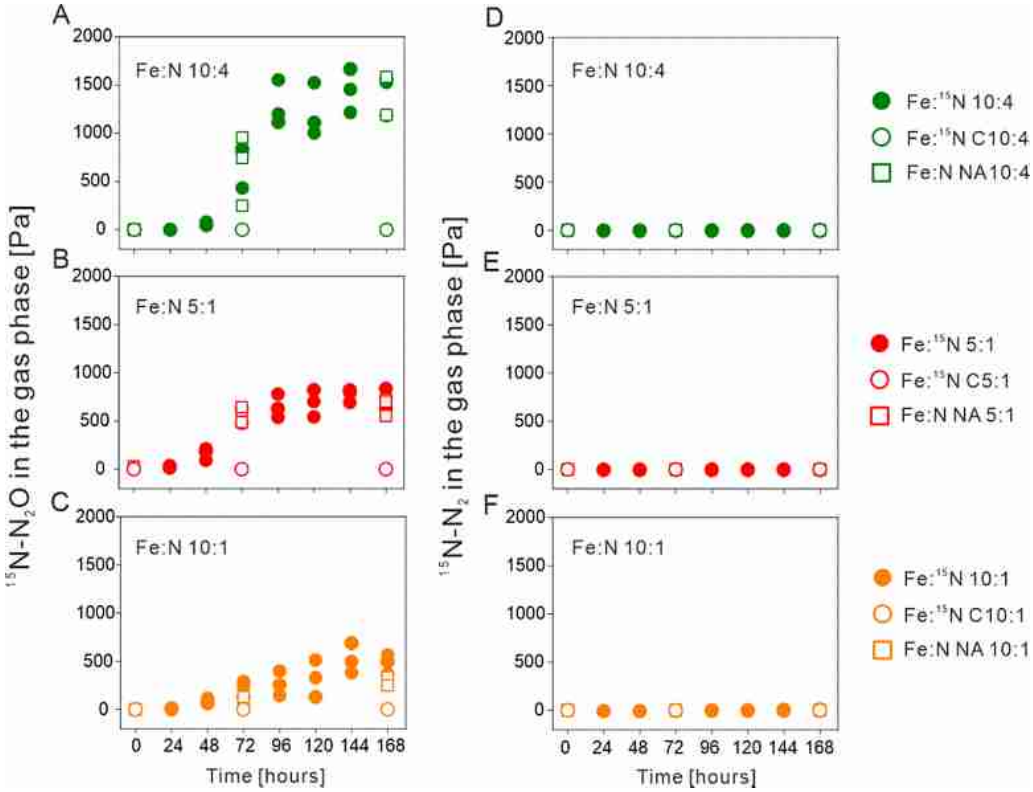

FIG 3 Time course changes of $^{15}N_2O$ (A to C) and $^{15}N_2$ (D to F) concentration in the gas phase by the autotrophic NRFeOx culture KS at three initial Fe/^{15}N ratios. C, control; NA, natural abundance.

However, the experimental ratios of oxidized Fe(II) to reduced nitrate in other autotrophic NRFeOx microorganisms were actually lower than 5, such as in culture BP (ratio of 3.4) (38), culture AG (ratio of 3.57) (9), and a marine sediment microcosm (ratio of 3.57 to 4.55) (8). We suggest two possible explanations for these observations. First, incomplete reduction of nitrate to intermediate N compounds such as NO or N_2O could lead to a decreased value for the ratio of $Fe(II)_{oxidized}$ to $nitrate_{reduced}$. Second, traces of organic carbon were present as a background contaminant in Milli-Q water used for preparation of cultivation medium. On one hand, this carbon may serve as electron donor [in addition to the Fe(II)] to reduce nitrate by heterotrophs, and this in turn will lower the ratio of oxidized Fe(II) to reduced nitrate. On the other hand, traces of organic carbon can be used as a carbon source to produce additional cells. A previous study from our lab calculated that 1 mg/L of dissolved organic carbon in Milli-Q water could in theory lead to the production of ca. 2.5×10^6 cells/mL (19). Therefore, it has to be considered that a fraction of the cells may not be produced via CO_2 fixation but may instead arise by using the traces of organic carbon from the water.

Despite both Fe(II) (e.g., ca. 5.6 mM at an Fe/N ratio of 10:1) and NO_3^- (e.g., ca. 2.2 mM at an Fe/N ratio of 10:4) being still present after 96 h, we did not observe any further Fe(II) oxidation and denitrification in culture KS. This observation was captured by our model and can be ascribed to a nonbioavailable fraction of Fe(II), i.e., Fe(II) phases that cannot be oxidized physiologically or thermodynamically by culture KS. It was suggested previously (37) that limited solubility of Fe(II) minerals could result in limited access of the cells to these minerals, preventing oxidation of the solid Fe(II).

We did not detect any quantifiable accumulation of nitrite during NRFO in our KS-inoculated batch experiments (Fig. S3B and E). This suggests that the second denitrification step is nonlimiting and that nitrite is quickly (relative to N_2O production) further reduced either by the cells or by an abiotic reaction of the nitrite with Fe(II). The transfer of NO_2^- and NO between the cells in culture KS would explain why nitrite is

efficiently reduced and does not accumulate (18). Furthermore, the absence of detected nitrite suggests the absence of a significant extent of abiotic Fe(II) oxidation by nitrite under autotrophic conditions (39). Alternatively, the competition for nitrite (and other N species) among the various strains could promote more efficient denitrification without nitrite accumulation and thus prevent abiotic Fe(II) oxidation (39). We have therefore omitted abiotic Fe(II) oxidation as a process contributing to nitrogen species reduction in our reaction model.

Influence of initial Fe(II) concentrations on Fe(III) minerals formed and cell-mineral interactions. At the end of our Fe(II) oxidation incubations, we observed visual differences between the colors of the mineral precipitates as a function of their initial Fe(II) concentration. Experiments at 10 mM were characterized by orange-brown precipitates, whereas those at 5 mM showed the formation of light green-brown minerals (Fig. S5). We hypothesize that the differences are driven by the initial proportions of vivianite, siderite, and dissolved Fe^{2+} in the freshwater mineral medium. During the preparation of the medium, the addition of Fe(II) led to the formation of a white-gray Fe(II)-rich precipitate, i.e., a mixture of poorly crystalline vivianite and siderite, stemming from the added Fe(II) and the phosphate (4.4 mM) and bicarbonate (22 mM), respectively, present in the mineral medium (15). Due to the presence of only low levels of dissolved phosphate after Fe(II) addition and the resulting Fe(II) mineral precipitation (less than 100 μM dissolved phosphate was measured in the 0.22-μm-filtered supernatant [Biao Wan, personal communication]) in all treatments, we hypothesize that almost all initial phosphate in the medium reacted with the added Fe(II) and formed vivianite (confirmed by MINEQL geochemical calculations [data not shown]). Therefore, in the 10 mM Fe(II) setups, approximately 4.3 mM vivianite plus a mixture of 5.7 mM dissolved Fe^{2+} and additional siderite existed in the medium, while in the 5 mM Fe(II) setups, the medium contained about 4.3 mM vivianite plus a mixture of 0.7 mM dissolved Fe^{2+} and additional siderite. At the end of Fe(II) oxidation, the initial whitish-gray precipitates became progressively brown-yellowish or greenish due to the oxidation of different proportions of Fe(II)-containing minerals in the medium, and the extent of the brown-yellowish color was further dependent on the concentrations of the remaining dissolved Fe^{2+} (Fig. S5). That means that the largest portion of the poorly crystalline Fe(II)-phosphate (i.e., vivianite) that was present initially was progressively oxidized to poorly crystalline Fe(III) phosphate and Fe(III) oxyhydroxides; the rest probably remained as (a small amount of) poorly crystalline Fe(II) phosphate (40).

When comparing the different setups with different concentrations of Fe(II) and nitrate, we found that the Fe/N ratios played a minor role in influencing the identity of microbially formed iron(III) minerals. Poorly crystalline minerals were the main Fe(III) phases produced by culture KS cultivated at all six initial Fe/N ratios (Fig. S7). The morphology of the spheroidal biogenic iron oxidation products was similar to that of ferrihydrite (41), as supported by the SEM-EDX results (Fig. S8). In contrast to our results, Cheng et al. (22) found that Fe/N ratios can play a critical role in Fe(III) mineral formation. In their pure-culture experiments with the mixotrophic NRFeOx bacterium *Paracoccus denitrificans*, they found that easily reducible oxyhydroxides (e.g., ferrihydrite) were the main Fe(III) minerals produced during NRFeOx at Fe/N ratios of 1:1 to 2:1, whereas goethite and ferrihydrite were both formed at Fe/N ratios of 3:1 to 10:1 (22). This difference could be due to the specific microbial strain in the experiments, that is, the enrichment culture KS versus a pure culture, nutrition modes (e.g., autotrophic versus mixotrophic), and/or the growth conditions (e.g., differences in pH, temperature, and presence of cell-derived organic matter) during NRFeOx (2, 42). Another possible reason for the presence of goethite in the mixotrophic culture could be the occurrence of abiotic Fe(II) oxidation induced by NO_2^- (the reactive intermediate product of nitrate reduction) during NRFeOx (6, 39, 43), which has been shown to produce goethite (32), whereas for KS, the absence of nitrite accumulation suggests that chemical Fe(II) oxidation by nitrite plays a negligible role in this culture.

In addition to the effects on Fe mineralogy, we were interested in whether the Fe(II) concentrations also influenced the interactions and associations between cells and the

newly formed Fe(III) minerals in culture KS. We found that the cells were closely associated with and partially encrusted by biogenic Fe(III) minerals at 10 mM Fe(II), whereas most cells were able to avoid encrustation and/or association with minerals at 5 mM Fe(II) (Fig. 2). The dependence of cell encrustation on Fe(II) concentrations and the lack thereof at lower Fe(II) concentrations were observed previously for the mixotrophic NRFeOx *Acidovorax* sp. strain 2AN (44). Most mixotrophic and some autotrophic NRFeOx bacteria face encrustation by Fe(III) minerals (2, 15, 17, 45), which may hinder the diffusion of nutrients and metabolites to the cells and waste products away from cells (41, 46).

Several possible mechanisms have been suggested as strategies used by cells to avoid encrustation, such as cell surface charge modification (41), excretion of Fe(III)-complexing ligands (47), and maintaining a slightly acidic microenvironment around Fe(II)-oxidizing cells (48). For the cells present in culture KS cultivated with 10 mM Fe(II), a certain fraction of them could not avoid the encrustation (and/or association with minerals). In contrast, we observed structural fibrils (mostly like EPS) closely associated with the Fe(III) minerals formed in culture KS cultivated with 5 mM Fe(II) (Fig. S6), which is consistent with a previous study (39). It has been suggested that EPS is produced as a stress reaction to protect the cells from encrustation (49). Thus, excretion of EPS could be a strategy for preventing encrustation and directing mineral formation away from the cells (50–53). Our data suggest that the extent of cell-mineral associations depends on Fe(II) concentrations in the autotrophic NRFeOx culture KS, and thus, the cells may develop different mechanisms to avoid cell encrustation.

Abundance of the genus *Gallionella*. The variations in initial Fe/N ratios had little effect on the community composition of the autotrophic NRFeOx enrichment culture KS. Our clone library analysis revealed that the genus *Gallionella* (family *Gallionellaceae*) was the dominating microorganism in culture KS at all initial Fe/N ratios tested here (Fig. S9). This suggests that the observed dominance of the family *Gallionellaceae* is a consequence of its chemolithoautotrophic lifestyle; that is, *Gallionella* can utilize dissolved inorganic carbon to build biomass (54), while the heterotrophic flanking community members depend on existing organic carbon in the growth medium. The experiments outlined here were not amended with organic carbon; thus, any organic carbon would have been a by-product of activity by members of the *Gallionellaceae*. Therefore, our experimental setup hindered the activity and kept the abundance of strains that require organic carbon low.

Incomplete denitrification and formation of N_2O in culture KS. Our KS cultivation experiments with ^{15}N-nitrate revealed that the denitrification process in the autotrophic NRFeOx culture KS is not complete at Fe(II)/nitrate ratios of 10:4, 5:1, and 10:1, even when the electron donor, i.e., Fe(II), is present in excess compared to the electron acceptor (i.e., nitrate). The main product of denitrification in culture KS was N_2O, while an almost negligible amount of N_2 was detected at the end of incubation (Fig. 3), demonstrating incomplete nitrate reduction. We attributed this incompleteness to a lack of genes coding for nitric oxide and nitrous oxide reductase in the family *Gallionellaceae* (the main contributor in culture KS), which are needed to reduce NO further to N_2 (18). While the flanking community strains theoretically can further reduce the N_2O to N_2, the lack of organic carbon (which was not amended and the only source was the organic carbon provided by the CO_2-fixing *Gallionellaceae*) probably explains why N_2O and not N_2 was the main end product. However, in the first study mentioning KS, this culture was reported to conduct complete denitrification and produce N_2 as the final product (1). This is likely because the heterotrophic flanking community (e.g., *Bradyrhizobium* sp., and *Rhodanobacter* sp.) in culture KS possesses all the reductases necessary for complete denitrification. The 1996 culture (and the current KS-Mad culture) likely contained a higher abundance of heterotrophic strains than the culture in the current study. Future research should aim to determine whether N_2O or N_2 is the final product of denitrification in culture KS-Mad.

Given the environmental importance of N_2O for the greenhouse gas budget, it is important to know how the Fe/N ratio controls the denitrification products (particularly N_2O emissions) during NRFO. Our geochemical analyses and ^{15}N isotope results showed that initial Fe(II) and nitrate values (i.e., the combination of both, the ratio, and

the absolute concentrations) play a key role in regulating N_2O emissions (Fig. S2; Fig. 3). First, the maximum amount of N_2O was produced at Fe/N ratios of 10:4 and 10:2, while it generally showed a decreasing tendency at higher Fe/N ratios of 10:1 to 10:0.5 (Fig. S2). This suggests that the critical ratio (5:1) of donor to acceptor [Fe(II) to nitrate] played a key role in controlling the amount of N_2O production. Second, the N_2O production at Fe/N ratios 10:4 and 10:2 was twice as high as at Fe/N ratios of 5:2 and 5:1, suggesting that the absolute concentrations had an influence on the concentrations of the denitrification products as well.

It must also be noted that 4.17 to 27.45%, 3.71 to 28.12%, and 33.74 to 56.87% of the added $^{15}NO_3^-$ were removed (not present as ^{15}N-nitrate anymore at the end) but not recovered as $^{15}N_2O$ or $^{15}N_2$ during autotrophic nitrate-reducing Fe(II) oxidation at Fe/^{15}N ratios of 10:4, 5:1, and 10:1, respectively (Fig. S11). Several processes could explain the fate of the missing nitrate: e.g., (i) nitrate may have been stored inside microbial cells or maybe also used as the N source for assimilation; (ii) nitrate could have been converted to NH_4^+ (dissimilatory nitrate reduction to ammonium [DNRA]), or (iii) nitrate could have been incompletely reduced to intermediate products such as NO. However, a rough calculation (see the supplemental material) showed that it is unlikely that a substantial amount of nitrate was removed by intracellular storage (55–57). Second, quantification of dissolved NH_4^+ showed that its overall concentration did not increase during the incubation (Fig. S3C and F), eliminating the possibility of DNRA taking place in culture KS. Finally, we saw that NO accumulated only at very low nanomolar levels (data not shown) in culture KS. Therefore, except for small analytical deviations during nitrate quantification in the microbial experiments, we cannot currently fully explain the reasons for the missing nitrate. Nevertheless, and most importantly, our findings indicated that denitrification during nitrate-reducing Fe(II) oxidation was incomplete in culture KS and the main N denitrification product was N_2O at the end of the experiment.

Electron balance. Rather than simulating a single growth rate for KS, we formulated separate cell division and biomass synthesis (driven by uptake of dissolved inorganic carbon [DIC]) rates in our reaction model (see Materials and Methods), guided by the observation that cell counts consistently increased before the measured increase in TOC. The latter suggests that culture KS cells multiply (divide) during nitrate reduction coupled to Fe(II) oxidation and that only thereafter do the newly produced daughter cells consume DIC [also coupled to Fe(II) oxidation] to produce more biomass. Our formulation accurately captured the increasing cell numbers during the incubations as well as the timing of the production of TOC. Considering both processes separately allowed us to track the allocation of electrons [that could stem only from Fe(II) in our setup] for both processes throughout the experiment. The cumulative proportion of electron uptake by either division or carbon assimilation and the electron consumption rate are presented as a function of time in Fig. 4. Our model clearly shows the effect of elevated Fe(II) concentrations on electron uptake. Both cell division and growth are delayed in the 10 mM Fe(II) incubations, relative to the timing in the 5 mM Fe(II) incubations, highlighting the effect of Fe(II) inhibition on the denitrification processes. Moreover, this model predicts that the partitioning of electrons between the energetic reaction and biomass buildup is consistent irrespective of the starting Fe(II) concentration and the Fe/N ratio. On average, our model, based on the concentration-time series measured, predicts that ca. 88% and 12% of the electrons are allocated to nitrate reduction and carbon assimilation, respectively. While our results are most likely relevant for environments with limited dissolved organic carbon (DOC), they are consistent with previously reported observations of 15% of electrons used for carbon fixation in autotrophic NRFeOx cultures (8) and 10% to 20% in other chemolithoautotrophs (58–61).

Conclusions and outlook. Our study provides a quantitative interpretation of the relative distribution of electrons to either biomass production or energy generation in the autotrophic NRFeOx culture KS, in which, on average, 12% of electrons went into biomass formation, while 88% of electrons were used for reduction of NO_3^- to N_2O. Based on this, it would be interesting to see whether the ratio of 12% versus 88% of electrons distributed to biomass formation and energy generation also holds true for the KS culture (KS-Mad) from

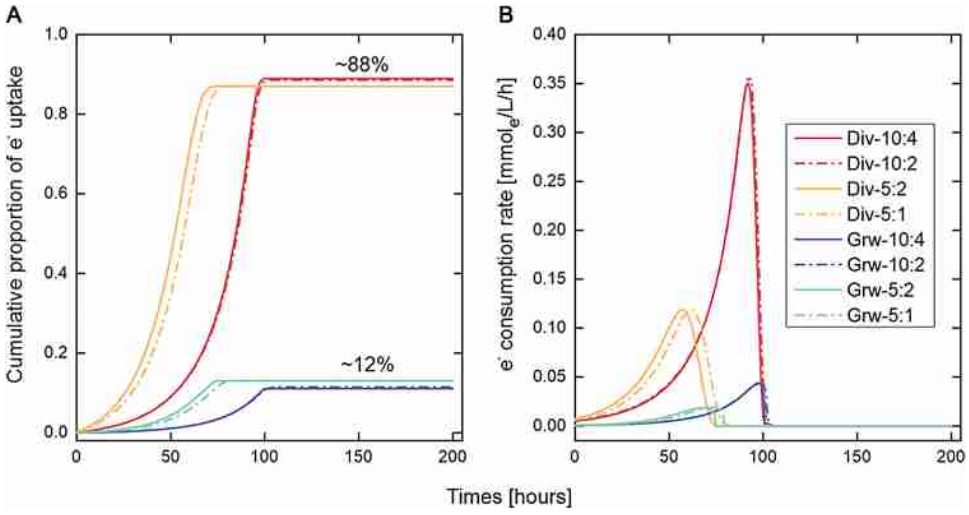

FIG 4 Cumulative relative proportion of electron uptake during all Fe/N (10:4, 10:2, 5:2, and 5:1) incubations, for electrons used in cell division (Div) (that is, the reduction of NO_3^- to N_2O) and electrons used in growth (Grw).

Eric Roden's lab (which has a different community composition and in particular a different content of the flanking community, which is able to reduce N_2O to N_2) and what these ratios look like for the other existing autotrophic cultures in general. Additionally, in the environment, at least small amounts of DOC are around in addition to Fe(II) and DIC. Further experiments are necessary to identify whether in such a case nitrate-reducing Fe(II)-oxidizing systems such as culture KS use more electrons from Fe(II) oxidation toward energy generation and/or use the DOC for biomass generation. Finally, it is also important to know whether the variation of the Fe(II) sources [with different redox potential of the electrons from the different Fe(II) compounds] would change the ratio of electron distribution in the autotrophic NRFeOx cultures; e.g., if electrons can be used to produce more energy because of a more favorable redox potential, then theoretically, fewer electrons [less Fe(II)] are needed for energy generation and more biomass can be produced.

MATERIALS AND METHODS

Source of microorganisms and microbial growth medium. Culture KS (culture KS-Tueb, referred to here as culture KS) is a chemolithoautotrophic, nitrate-reducing Fe(II)-oxidizing enrichment culture that was originally isolated from a ditch in Bremen, Germany, and has been cultivated in our laboratory for several years. Before the experiments, culture KS was cultivated in an anoxic bicarbonate-buffered (22 mM) freshwater mineral medium modified from the work of Ehrenreich and Widdel (62). The freshwater mineral medium (pH 6.8 to 7.0), containing 0.6 g/L KH_2PO_4, 0.3 g/L NH_4Cl, 0.5 g/L $MgSO_4 \cdot 7H_2O$, and 0.1 g/L $CaCl_2 \cdot 2H_2O$, was autoclaved and cooled. Filter-sterilized non-chelated trace element mixture SL10 (1 mL/L), 7-vitamin solution (1 mL/L), and selenite-tungstate solution (1 mL/L) were added (63). Serum bottles (100 mL) were filled anoxically with 50 mL of the above-mentioned medium. The bottles were sealed with butyl rubber stoppers and crimped with aluminum caps, and the headspace was flushed with N_2-CO_2 (90:10 [vol/vol]) gas. For routine cultivation of culture KS, 10 mM $FeCl_2$, 4 mM $NaNO_3$ and 1% (vol/vol) inoculum were added to the freshwater mineral medium under autotrophic conditions and incubated in the dark at 28°C. After Fe(II) addition, a whitish-gray precipitate formed in the medium, suggesting the formation of siderite and vivianite due to the phosphate and bicarbonate present in the medium (15).

Experiment setups and chemical analyses. To investigate the relative contributions of electrons to CO_2 fixation and nitrate reduction as well as the metabolic performance of autotrophic NRFeOx culture KS grown at different initial Fe/N ratios, 12 batch treatments were conducted as follows (Fig. S12A and B). Six biotic treatments were set up with $FeCl_2$ and $NaNO_3$ concentrations of 10 and 4 mM, 10 and 2 mM, 10 and 1 mM, 5 and 2 mM, 5 and 1 mM, and 10 and 0.5 mM, resulting in initial Fe/N ratios of 10:4, 10:2, 10:1, 5:2, 5:1, and 10:0.5, respectively. Although the Fe(II):nitrate ratios of 10:4 and 5:2 represented the same ratio of electron donor to electron acceptor, the absolute concentrations of the substrates were different (in the case of the ratio 10:4, twice as high as at the ratio of 5:2) and, as we observed in the results, had a different influence on NRFeOx performance (the denitrification products) in our experiments. Therefore, six different initial Fe/N ratios were chosen for this study. After this step, the bottles were inoculated with 1% (vol/vol) (0.5 mL of each bottle, ca. 3.5×10^5 cells/mL initially in the freshly inoculated bottle) of a 120-h old preculture grown at 28°C on 10 mM $FeCl_2$ and 4 mM $NaNO_3$. Simultaneously, six sterile setups (killed cells) with the same Fe/N ratios were used as abiotic treatments. Killed cells were obtained by heating in a water bath at 80°C for 30 min. All trials were conducted in triplicate, and samples were incubated at 28°C in the dark.

At 0, 24, 48, 72, 96, 120, 144 and 168 h, samples (0.7 mL) were taken from the serum bottles in an anoxic glove box (100% N_2) using a syringe with a needle through the butyl-rubber stopper. Thereafter, the samples were used to quantify the concentrations of Fe(II), Fe(tot), NO_3^-, NO_2^-, and N_2O, as well as cell numbers (Fig. S12C). For N_2O quantification, 0.3 mL headspace gas of each serum bottle was sampled using a Hamilton syringe and transferred into 22-mL vials previously flushed with helium. The N_2O concentration was measured by a gas chromatograph with a pulsed discharge detector (PDD). The back PDD used was a Molsieb5a 30-m by 0.53-mm-inner-diameter (ID) instrument, and the front PDD was a TG BondQ+ 30-m by 0.25-mm-ID instrument. For quantification of Fe(II) and Fe(tot) concentrations, we used the revised ferrozine protocol for nitrite-containing samples as described earlier (43, 64). The purple ferrozine-Fe(II) complex was quantified at 562 nm using a microtiter plate reader (FlashScan 550; Analytik Jena, Germany). All ferrozine measurements were done in triplicate. For NO_3^- and NO_2^- measurements, samples were centrifuged at 13,400 $\times$ *g* for 5 min to remove cells and minerals and were diluted with anoxic Milli-Q water before analysis (Fig. S12C). The concentrations of NO_3^-, NO_2^-, and NH_4^+ were quantified by using a flow injection analysis (FIA) system (3-QuAAtro; Bran+Lübbe, Norderstedt, Germany). The system was equipped with a dialysis membrane for Fe removal to prevent side reactions during analysis. A 0.3-mL sample suspension was used for cell counts. Prior to cell counts, a mineral dissolution step was conducted (38). Then, cells were stained with BacLight Green stain (Thermo Fisher Scientific), and cell numbers were determined in triplicate with an Attune NxT flow cytometer (Thermo Fisher Scientific) with the instrument setup adapted from the procedure described previously (38). For quantification of TOC contents, 12 batch treatments were prepared in parallel as described above (Fig. S12C). At each sampling point, samples (1.5 mL) were taken from the serum bottle under sterile conditions and were diluted with medium if necessary. Prior to analysis, the sample was acidified with 50 μL of 2 M HCl and flushed with O_2 to remove inorganic and purgeable organic carbon. Each TOC sample was measured in triplicate as the nonpurgeable organic carbon. The nonpurgeable organic carbon in 100 μL of sample was analyzed by combustion at 750°C and detection by nondispersive infrared absorption selective for CO_2 (Multi N/C analyzer 2100S; Analytik Jena GmbH).

DNA extraction, PCR amplification, and clone library construction. Genomic DNA from the enrichment culture KS cultivated at six Fe/N ratios (ca. 120 h old, stationary phase) was extracted with a DNeasy UltraClean microbial kit (Qiagen, Germany) according to the manufacturer's instructions. The 16S rRNA gene of the extracted DNA was amplified with the general primers 341f (5′-CCTACGGGAGGC AGCAG-3′) and 907r (5′-CCGTCAATTCCTTTRAGTTT-3′) (65). PCR amplification was performed in a 25-μL reaction mixture containing 1 μL of DNA template (1 to 20 ng/μL), 5 μL of 5$\times$ Go *Taq* reaction buffer, 1 μL of $MgCl_2$ (Promega), 0.5 μL of deoxynucleoside triphosphate (dNTP) mix (New England Biolabs), 0.5 μL of each primer, 0.125 μL Go *Taq* polymerase (Promega), and 16.375 μL of double-distilled water. Conditions for the PCR program were as follows: initial denaturation at 95°C for 5 min; 25 cycles of denaturation at 95°C for 30 s, annealing at 45°C for 30 s, and extension at 72°C for 90 s; and the final elongation step at 72°C for 8 min 30 s. The triplicate PCR products were purified with the Wizard SV gel and PCR clean-up system (Promega, USA). The quality and quantity of cleaned PCR products were checked with an Agilent 2100 bioanalyzer system (Agilent, USA). To obtain a detailed identification of microbial community members of culture KS cultivated at different initial Fe/N ratios, small clone libraries containing 16S rRNA fragments were constructed. The resulting purified PCR products were ligated into the pDrive vector system (Qiagen, Germany). Then the ligation products were transformed into *Escherichia coli* DH5α competent cells, and the transformed cells were spread on LB (with ampicillin, isopropyl-β-D-thiogalactopyranoside [IPTG], and 5-bromo-4-chloro-3-indolyl-β-D-galactopyranoside [X-Gal]) agar plates for blue-white screening. The white colonies of each constructed gene library were randomly selected, PCR screened, and sent for sequencing of the 16S rRNA gene insert to GATC Biotech (Constance, Germany). Forward and reverse reads were assembled and trimmed using the BioEdit program (DNAStar software). The sequences after trimming (~550 bp) were aligned and analyzed with the reference sequences in the NCBI GenBank database and with type strains of validly named species retrieved from EzBioCloud (http://www.ezbiocloud.net/).

XRD, SEM, and EDX. Suspended mineral precipitates (approximately 20 mL) of enrichment culture KS cultivated at different initial Fe/N ratios were withdrawn with sterile syringes and were centrifuged at 13,400 $\times$ *g* for 10 min in an anoxic glove box (100% N_2). The supernatant was discarded, and the precipitates were dried anoxically for several days in the glove box. The minerals in the precipitates were analyzed with an X-ray diffractometer (Bruker D8 Discover with general area detector diffraction system (GADDS), XRD^2 method) using Co Kα filtered radiation (λ = 0.17903 nm) at parameters of 30 kV and 30 mA. The precipitate samples were scanned between 10° and 65° 2θ using a step size of 0.05°. The obtained data were analyzed with the software Match! (version 3.6.2.121) to identify the mineral phases.

SEM was used to visualize the cell-mineral interactions during nitrate-reducing Fe(II) oxidation by enrichment culture KS cultivated at different initial Fe/N ratios. Culture suspension (1 mL per sample) was withdrawn with a syringe in the glove box (100% N_2) after 120 h of cultivation. Outside the glove box, each sample (900 μL) was fixed with 2.5% glutaraldehyde (100 μL) and left at 4°C overnight. Stepwise dehydration was performed by an ethanol dilution series (30% ethanol for 5 min, 75% ethanol for 5 min, 95% ethanol for 5 min, and 100% ethanol for 30 min twice) before incubation in hexamethyldisilazane (HMDS; Sigma-Aldrich, St. Louis, MO, USA) (66). The samples were coated with an ~8-nm Pt layer using a BAL-TEC SCD 500 sputter coater before imaging. The micrographs of cells and precipitates were collected at the Tübingen Structural Microscopy Core Facility, University of Tübingen, using a Zeiss Crossbeam 550L FIB-SEM (working distance, 4.0 mm; acceleration voltage, 2.00 kV). For each setup, more than 20 cells were analyzed and a representative scanning electron micrograph was selected for presentation. The elemental composition of the resulting precipitates was further examined by an Oxford EDX detector (UltimMax 100) (working distance, 5.0 mm; acceleration voltage, 20 kV) and AZtecEnergy Advanced software.

^{15}N isotope experiments. To analyze the gaseous products of nitrate reduction coupled to Fe(II) oxidation during growth of the autotrophic NRFeOx enrichment culture KS, an isotopic tracing experiment with ^{15}N-labeled $NaNO_3$ was performed. The experimental setup was run using the same medium, substrate, and inoculum volume (1% [vol/vol]), except that the medium was amended with ^{15}N-labeled $NaNO_3$ and the incubation volume was reduced by half (50 mL to 25 mL) (Fig. S13A). For the isotopic tracing experiments with ^{15}N-labeled $NaNO_3$, only three batch treatments were conducted, with Fe/^{15}N ratios of 10:4, 5:1, and 10:1. Additionally, two sets of controls were run. In one set (abiotic control), microbial activity was inhibited by heating in a water bath at 80°C for 30 min. A second control (unlabeled control) was prepared using unlabeled $NaNO_3$ to reveal the natural abundance (NA) of isotopes. The sacrificial sampling method was used in the labeled experiment, and all setups were run in triplicate. At each sampling point (all the biotic samples at 8 time points, abiotic samples at 3 time points [0, 72, and 168 h], and samples from unlabeled incubations at 3 time points [0 h, 72 h, and 168 h]), the bottles were sacrificed, and the entire volume of the headspace (25 mL) was withdrawn from each bottle using a Hamilton gas-tight syringe and injected into a crimped serum vial with a rubber butyl stopper that had been prefilled with He (Fig. S13B). Hence, all N_2O and N_2 in the headspace of these vials stemmed from the experimental bottles, and there was no dilution of N_2 from the atmosphere. The samples were further analyzed using gas chromatography-mass spectrometry (GC-MS). The kinetic experiments with ^{15}N-labeled $NaNO_3$ were set up in parallel (Fig. S13C) and were done as described above. Therefore, besides $^{15}N_2$ and $^{15}N_2O$, Fe(II), Fe(tot), $^{15}NO_3^-$, and $^{15}NO_2^-$ were also analyzed (Fig. S13D).

The detailed procedures of GC-MS analysis, quantification of N_2 from denitrification, and quantification of N_2O from denitrification were performed as reported previously (9). Briefly, quantification of N_2 and N_2O was performed on an Agilent 7890A GC coupled to an Agilent 5975C quadrupole MS in electron impact mode. Signals at *m/z* 28, 29, and 30 (for N_2) and *m/z* 44, 45, and 46 (for N_2O) were acquired in selected ion monitoring (SIM) mode with a dwell time of 100 ms for each signal. All MS parameters were obtained by standard autotuning using perfluorotributylamine (PFTBA) at *m/z* 69, 219, and 502. The calculation of the partial pressure of N_2O (in pascals) is shown in the next section. The concentrations of N_2 and N_2O from denitrification were evaluated following the equations proposed by Jakus and colleagues (9). Finally, the nitrogen transformed from $NaNO_3$ to both N_2 and N_2O was calculated as follows:

$$p(\mathrm{N}_{\text{trans. to } \mathrm{N_2}}) = \frac{2 \times [^{30}\mathrm{N_2}]_{\text{denitrification}}}{[\mathrm{NaNO_3}]} \times 100 \tag{2}$$

$$p(\mathrm{N}_{\text{trans. to } \mathrm{N_2O}}) = \frac{2 \times [\mathrm{N_2O}]}{[\mathrm{NaNO_3}]} \times 100 \tag{3}$$

where $[^{30}N_2]_{\text{denitrification}}$ and $[N_2O]$ refer to the amount of substance formed by denitrification and $[NaNO_3]$ refers to the initial amount of $NaNO_3$ added to the medium.

Numerical modeling. For quantification of the electron balance between biomass production (CO_2 fixation) and energy generation (nitrate reduction) by autotrophic NRFeOx culture KS cultivated at different initial Fe/N ratios, we formulated a reaction model to fit the kinetic results collected from our incubation experiments. The denitrification process is a chain of reactions starting with the reduction of nitrate and with the final product of dinitrogen ($NO_3^- \rightarrow NO_2^- \rightarrow NO \rightarrow N_2O \rightarrow N_2$). Based on our observations that no NO_2^- accumulated in our batch experiments as a reactive intermediate and that no labeled $^{15}NO_3^-$ was reduced to N_2, we formulated a denitrification model that considered a single reduction step from nitrate to nitrous oxide ($NO_3^- \rightarrow N_2O$). We decoupled the energy and growth metabolisms by distinguishing between cell division and biomass synthesis, the latter referring to the formation of new biomass after the cells had divided.

$$r_{\text{div}} = \mu_{\max}\left(\frac{C_{NO_3^-}}{C_{NO_3^-} + K_{NO_3^-}}\right)\left(\frac{C_{Fe^{2+}}}{C_{Fe^{2+}} + K_{Fe^{2+}}}\right)\left(\frac{K_{I,Fe^{2+}}}{C_{Fe^{2+}} + K_{I,Fe^{2+}}}\right)X \tag{4}$$

Equation 4 was used to calculate the rate of cell division, r_{div} (cells per liter per hour), in which $\mu_{\max}$ (per hour) is the maximum specific growth rate constant, $C_{NO_3^-}$ and $C_{Fe^{2+}}$ (millimolar units) are the aqueous (bioavailable) concentrations of nitrate and ferrous iron, $K_{NO_3^-}$ and $K_{Fe^{2+}}$ (millimolar units) are their respective half-saturation constants, $K_{I,Fe^{2+}}$ (millimolar units) denotes the inhibition concentration of Fe(II), and X (cells per liter) is the cell density. The third term in brackets in equation 4 is an inhibition term that captures the well-documented inhibition of microbial growth rates in the presence of high concentrations of Fe(II) (39). Bioavailable Fe(II) was computed as the difference between the actual available amount and a threshold concentration ($C_{Fe^{2+}} = C_{Fe^{2+}}{}^{\text{tot}} - C_{Fe^{2+}}{}^{\text{thresh}}$) (37), based on the observation that Fe(II) was not fully consumed in any of the experiments.

We formulated a rate of biomass synthesis, r_{upt} (millimoles of C per liter per hour), where newly divided daughter cells take up inorganic carbon and reduce it to form organic biomass (their own cell structure), coupled to the oxidation of Fe(II):

$$r_{\text{upt}} = k_{\text{upt}} X\left(\frac{C_{Fe^{2+}}}{C_{Fe^{2+}} + K_{\text{upt}}^{Fe^{2+}}}\right) \tag{5}$$

in which k_{upt} (millimoles of C per cell per hour) is the carbon uptake rate constant per cell and $K_{\text{upt}}^{Fe^{2+}}$ (millimolar units) denotes the half-saturation constant for Fe(II) oxidation coupled to inorganic carbon

reduction to biomass. The density of cells changes as a function of cell division and decay (decay rate coefficient is denoted by k_{decay} [per hour]), whereas the uptake rate influences the amount of TOC, that is, organic biomass:

$$\frac{dX}{dt} = r_{div} - k_{decay}X \tag{6}$$

$$\frac{d\mathrm{TOC}}{dt} = r_{upt} \tag{7}$$

The division and biomass synthesis reactions yield the following system of governing equations for concentration and partial pressure changes of chemical species in the aqueous and gaseous phases, respectively:

$$\frac{dC_{Fe^{2+}}}{dt} = -\frac{r_{div}}{Y} + 4r_{upt} \tag{8}$$

$$\frac{dC_{NO_3^-}}{dt} = -\frac{1}{4}\frac{r_{div}}{Y} \tag{9}$$

$$\frac{dC_{N_2O}}{dt} = \frac{1}{8}\frac{r_{div}}{Y} - \lambda\left(C_{N_2O} - \frac{p_{N_2O}}{RT}H\right) \tag{10}$$

$$\frac{dp_{N_2O}}{dt} = \frac{V_w}{V_g}\lambda\left(\frac{p_{N_2O}}{RT} - \frac{C_{N_2O}}{H}\right)RT - f_{dil}k_{sample}p_{N_2O} \tag{11}$$

The rate expressions in equations 8 to 11 are multiplied by their corresponding stoichiometric coefficients. The yield coefficient, Y, is expressed per unit of electron donor [cells per mole of Fe(II)]. Nitrous oxides are modeled as a volatile compound that can partition between aqueous and gaseous phases. The partitioning was achieved via first-order linear driving force mass transfer approximation, where p_{N_2O} is the partial pressure of N_2O (pascals), λ (per hour) is the first-order exchange coefficient, and H, R (joules per mole per Kelvin), and T (Kelvin) are the Henry's law coefficient for N_2O, the ideal gas constant, and temperature, respectively ($H = C_{aq}/C_g$). The dilution of partial pressure driven by periodic sampling events was accounted for via a first-order sampling rate, k_{sample} (per hour), scaled by the fraction of gas exchanged at each sampling event, f_{dil} (67). The system of equations was solved in Matlab using the integrated ode-solver function ode15s. Parameter estimation was performed by fitting all experiments jointly using the trust region-reflective algorithm (68), minimizing the sum of squared error between measured data and model output. For a summary of model parameter values, the reader is referred to the supplemental material. Note that the highest Fe/N ratios, 10:1 and 10:0.5 (in particular the data obtained with 0.5 mM nitrate), were not simulated, because these low-nitrate-concentration processes were not reflected by our model simulation. As a result, our reaction model for Fe(II) oxidation, nitrate reduction, and biomass production was successfully simulated at four Fe/N ratios (10:4, 10:2, 5:2, and 5:1).

Data availability. All sequencing data obtained from the clone library have been deposited in the GenBank database under the accession numbers ON799274 to ON799332.

SUPPLEMENTAL MATERIAL

Supplemental material is available online only.

SUPPLEMENTAL FILE 1, PDF file, 3.2 MB.

ACKNOWLEDGMENTS

A.K. acknowledges infrastructural support by the Deutsche Forschungsgemeinschaft (DFG, German Research Foundation) under Germany's Excellence Strategy, cluster of Excellence EXC2124, project ID 390838134. This work was also supported by grants from the National Natural Science Foundation of China (grant no. 42202338), and the China Scholarship Council (CSC).

We thank Franziska Schaedler for nitrate/nitrite/ammonium analyses and clone library construction, Hanna Grimm for TOC measurements, Soeren Drabesch for N_2O gas measurements, Stefanie Becker and Verena Nikeleit for help with the flow cytometer, and Biao Wan for phosphorus measurements. We gratefully acknowledge the Tübingen Structural Microscopy Core Facility (funded by the Excellence Strategy of the German Federal and State Governments) for their support and assistance in this work.

We declare that we have no conflict of interest.

REFERENCES

1. Straub KL, Benz M, Schink B, Widdel F. 1996. Anaerobic, nitrate-dependent microbial oxidation of ferrous iron. Appl Environ Microbiol 62:1458–1460. https://doi.org/10.1128/AEM.62.4.1458-1460.1996.
2. Kappler A, Bryce C, Mansor M, Lueder U, Byrne JM, Swanner ED. 2021. An evolving view on biogeochemical cycling of iron. Nat Rev Microbiol 19:360–374. https://doi.org/10.1038/s41579-020-00502-7.
3. Bryce C, Blackwell N, Schmidt C, Otte J, Huang Y-M, Kleindienst S, Tomaszewski E, Schad M, Warter V, Peng C, Byrne JM, Kappler A. 2018. Microbial anaerobic Fe (II) oxidation - ecology, mechanisms and environmental implications. Environ Microbiol 20:3462–3483. https://doi.org/10.1111/1462-2920.14328.
4. Weber KA, Achenbach LA, Coates JD. 2006. Microorganisms pumping iron: anaerobic microbial iron oxidation and reduction. Nat Rev Microbiol 4:752–764. https://doi.org/10.1038/nrmicro1490.
5. Liu T, Chen D, Li X, Li F. 2019. Microbially mediated coupling of nitrate reduction and Fe(II) oxidation under anoxic conditions. FEMS Microbiol Ecol 95:fiz030. https://doi.org/10.1093/femsec/fiz030.
6. Cheng B, Hua Y, Zhao J, Liu G, Wan X. 2020. Nitrogen transformation mediated by nitrate-dependent iron oxidation in anoxic freshwater. J Soils Sediments 20:1087–1096. https://doi.org/10.1007/s11368-019-02461-w.
7. Weber KA, Pollock J, Cole KA, O'Connor SM, Achenbach LA, Coates JD. 2006. Anaerobic nitrate-dependent iron (II) bio-oxidation by a novel lithoautotrophic betaproteobacterium, strain 2002. Appl Environ Microbiol 72:686–694. https://doi.org/10.1128/AEM.72.1.686-694.2006.
8. Laufer K, Røy H, Jørgensen BB, Kappler A. 2016. Evidence for the existence of autotrophic nitrate-reducing Fe(II)-oxidizing bacteria in marine coastal sediment. Appl Environ Microbiol 82:6120–6131. https://doi.org/10.1128/AEM.01570-16.
9. Jakus N, Blackwell N, Osenbrück K, Straub D, Byrne JM, Wang Z, Glöckler D, Elsner M, Lueders T, Grathwohl P, Kleindienst S, Kappler A. 2021. Nitrate removal by a novel lithoautotrophic nitrate-reducing iron (II)-oxidizing culture enriched from a pyrite-rich limestone aquifer. Appl Environ Microbiol 87:e00460-21. https://doi.org/10.1128/AEM.00460-21.
10. Hafenbradl D, Keller M, Dirmeier R, Rachel R, Rossnagel P, Burggraf S, Huber H, Stetter KO. 1996. *Ferroglobus placidus* gen. nov., sp. nov., a novel hyperthermophilic archaeum that oxidizes Fe^{2+} at neutral pH under anoxic conditions. Arch Microbiol 166:308–314. https://doi.org/10.1007/s002030050388.
11. Mattes A, Gould D, Taupp M, Glasauer S. 2013. A novel autotrophic bacterium isolated from an engineered wetland system links nitrate-coupled iron oxidation to the removal of As, Zn and S. Water Air Soil Pollut 224:1490. https://doi.org/10.1007/s11270-013-1490-8.
12. Li B, Tian C, Zhang D, Pan X. 2014. Anaerobic nitrate-dependent iron (II) oxidation by a novel autotrophic bacterium, *Citrobacter freundii* strain PXL1. Geomicrobiol J 31:138–144. https://doi.org/10.1080/01490451.2013.816393.
13. Ratering S, Schnell S. 2001. Nitrate-dependent iron(II) oxidation in paddy soil. Environ Microbiol 3:100–109. https://doi.org/10.1046/j.1462-2920.2001.00163.x.
14. Blöthe M, Roden EE. 2009. Composition and activity of an autotrophic Fe(II)-oxidizing, nitrate-reducing enrichment culture. Appl Environ Microbiol 75:6937–6940. https://doi.org/10.1128/AEM.01742-09.
15. Kappler A, Schink B, Newman DK. 2005. Fe(III) mineral formation and cell encrustation by the nitrate-dependent Fe(II)-oxidizer strain BoFeN1. Geobiology 3:235–245. https://doi.org/10.1111/j.1472-4669.2006.00056.x.
16. Dopffel N, Jamieson J, Bryce C, Joshi P, Mansor M, Siade A, Prommer H, Kappler A. 2022. Temperature dependence of nitrate-reducing Fe(II) oxidation by *Acidovorax* strain BoFeN1 - evaluating the role of enzymatic vs. abiotic Fe(II) oxidation by nitrite. FEMS Microbiol Ecol 97:fiab155. https://doi.org/10.1093/femsec/fiab155.
17. Huang J, Han M, Yang J, Kappler A, Jiang H. 2022. Salinity impact on composition and activity of nitrate-reducing Fe(II)-oxidizing microorganisms in saline lakes. Appl Environ Microbiol 88:e00132-22. https://doi.org/10.1128/aem.00132-22.
18. He S, Tominski C, Kappler A, Behrens S, Roden EE. 2016. Metagenomic analyses of the autotrophic Fe(II)-oxidizing, nitrate-reducing enrichment culture KS. Appl Environ Microbiol 82:2656–2668. https://doi.org/10.1128/AEM.03493-15.
19. Huang Y-M, Straub D, Blackwell N, Kappler A, Kleindienst S. 2021. Metaomics reveal *Gallionellaceae* and *Rhodanobacter* as interdependent key players for Fe(II) oxidation and nitrate reduction in the autotrophic enrichment culture KS. Appl Environ Microbiol 87:e00496-21. https://doi.org/10.1128/AEM.00496-21.
20. Deng S, Peng S, Ngo HH, Oh SJ-A, Hu Z, Yao H, Li D. 2022. Characterization of nitrous oxide and nitrite accumulation during iron (Fe(0))- and ferrous iron (Fe(II))-driven autotrophic denitrification: mechanisms, environmental impact factors and molecular microbial characterization. Chem Eng J 438:135627. https://doi.org/10.1016/j.cej.2022.135627.
21. Sparacino-Watkins C, Stolz JF, Basu P. 2014. Nitrate and periplasmic nitrate reductases. Chem Soc Rev 43:676–706. https://doi.org/10.1039/C3CS60249D.
22. Cheng B, Wang Y, Hua Y, Heal KV. 2021. The performance of nitrate-reducing Fe(II) oxidation processes under variable initial Fe/N ratios: the fate of nitrogen and iron species. Front Environ Sci Eng 15:73. https://doi.org/10.1007/s11783-020-1366-2.
23. Wolfe AH, Patz JA. 2002. Reactive nitrogen and human health: acute and long-term implications. Ambio 31:120–125. https://doi.org/10.1579/0044-7447-31.2.120.
24. Stamler JS, Singel DJ, Loscalzo J. 1992. Biochemistry of nitric oxide and its redox-activated forms. Science 258:1898–1902. https://doi.org/10.1126/science.1281928.
25. Mellage A, Smeaton CM, Furman A, Atekwana EA, Rezanezhad F, Van Cappellen P. 2019. Bacterial Stern layer diffusion: experimental determination with spectral induced polarization and sensitivity to nitrite toxicity. Near Surf Geophys 17:623–635. https://doi.org/10.1002/nsg.12058.
26. Sijbesma WFH, Almeida JS, Reis MAM, Santos H. 1996. Uncoupling effect of nitrite during denitrification by *Pseudomonas fluorescens*: an in vivo ^{31}P-NMR study. Biotechnol Bioeng 52:176–182. https://doi.org/10.1002/(SICI)1097-0290(19961005)52:1%3C176::AID-BIT18%3E3.0.CO;2-M.
27. Saini G. 2014. Metabolic uncoupling: biomass control strategy in microbial processes. J Microb Biochem Technol 6:e117. https://doi.org/10.4172/1948-5948.1000e117.
28. Ravishankara AR, Daniel JS, Portmann RW. 2009. Nitrous oxide (N_2O): the dominant ozone-depleting substance emitted in the 21st century. Science 326:123–125. https://doi.org/10.1126/science.1176985.
29. Massara TM, Malamis S, Guisasola A, Baeza JA, Noutsopoulos C, Katsou E. 2017. A review on nitrous oxide (N_2O) emissions during biological nutrient removal from municipal wastewater and sludge reject water. Sci Total Environ 596–597:106–123. https://doi.org/10.1016/j.scitotenv.2017.03.191.
30. Margalef-Marti R, Carrey R, Benito JA, Marti V, Soler A, Otero N. 2020. Nitrate and nitrite reduction by ferrous iron minerals in polluted groundwater: isotopic characterization of batch experiments. Chem Geol 548:119691. https://doi.org/10.1016/j.chemgeo.2020.119691.
31. Scherson YD, Wells GF, Woo S-G, Lee J, Park J, Cantwell BJ, Criddle CS. 2013. Nitrogen removal with energy recovery through N_2O decomposition. Energy Environ Sci 6:241–248. https://doi.org/10.1039/C2EE22487A.
32. Chen D, Liu T, Li X, Li F, Luo X, Wu Y, Wang Y. 2018. Biological and chemical processes of microbially mediated nitrate-reducing Fe(II) oxidation by *Pseudogulbenkiania* sp. strain 2002. Chem Geol 476:59–69. https://doi.org/10.1016/j.chemgeo.2017.11.004.
33. Wang M, Hu R, Zhao J, Kuzyakov Y, Liu S. 2016. Iron oxidation affects nitrous oxide emissions via donating electrons to denitrification in paddy soils. Geoderma 271:173–180. https://doi.org/10.1016/j.geoderma.2016.02.022.
34. Zhang M, Zheng P, Wang R, Li W, Lu H, Zhang J. 2014. Nitrate-dependent anaerobic ferrous oxidation (NAFO) by denitrifying bacteria: a perspective autotrophic nitrogen pollution control technology. Chemosphere 117:604–609. https://doi.org/10.1016/j.chemosphere.2014.09.029.
35. Kiskira K, Papirio S, van Hullebusch ED, Esposito G. 2017. Fe(II)-mediated autotrophic denitrification: a new bioprocess for iron bioprecipitation/biorecovery and simultaneous treatment of nitrate-containing wastewaters. Int Biodeterior Biodegrad 119:631–648. https://doi.org/10.1016/j.ibiod.2016.09.020.
36. Tominski C, Heyer H, Lösekann-Behrens T, Behrens S, Kappler A. 2018. Growth and population dynamics of the anaerobic Fe(II)-oxidizing and nitrate-reducing enrichment culture KS. Appl Environ Microbiol 84:e02173-17. https://doi.org/10.1128/AEM.02173-17.
37. Jakus N, Mellage A, Höschen C, Maisch M, Byrne JM, Mueller CW, Grathwohl P, Kappler A. 2021. Anaerobic neutrophilic pyrite oxidation by a chemolithoautotrophic nitrate-reducing iron(II)-oxidizing culture enriched from a fractured aquifer. Environ Sci Technol 55:9876–9884. https://doi.org/10.1021/acs.est.1c02049.
38. Huang Y-M, Straub D, Kappler A, Smith N, Blackwell N, Kleindienst S. 2021. A novel enrichment culture highlights core features of microbial networks contributing to autotrophic Fe(II) oxidation coupled to nitrate reduction. Microb Physiol 31:280–295. https://doi.org/10.1159/000517083.
39. Nordhoff M, Tominski C, Halama M, Byrne J, Obst M, Kleindienst S, Behrens S, Kappler A. 2017. Insights into nitrate-reducing Fe(II) oxidation mechanisms through analysis of cell-mineral associations, cell encrustation, and mineralogy in the chemolithoautotrophic enrichment culture KS. Appl Environ Microbiol 83:e00752-17. https://doi.org/10.1128/AEM.00752-17.

40. Miot J, Benzerara K, Morin G, Bernard S, Beyssac O, Larquet E, Ona-Nguema G, Kappler A, Guyot F. 2009. Transformation of vivianite by anaerobic nitrate-reducing iron-oxidizing bacteria. Geobiology 7:373–384. https://doi.org/10.1111/j.1472-4669.2009.00203.x.
41. Schädler S, Burkhardt C, Hegler F, Straub KL, Miot J, Benzerara K, Kappler A. 2009. Formation of cell-iron-mineral aggregates by phototrophic and nitrate-reducing anaerobic Fe(II)-oxidizing bacteria. Geomicrobiol J 26:93–103. https://doi.org/10.1080/01490450802660573.
42. Larese-Casanova P, Kappler A, Haderlein SB. 2012. Heterogeneous oxidation of Fe(II) on iron oxides: controls on Fe(III) product formation. Geochim Cosmochim Acta 91:171–186. https://doi.org/10.1016/j.gca.2012.05.031.
43. Klueglein N, Kappler A. 2013. Abiotic oxidation of Fe(II) by reactive nitrogen species in cultures of the nitrate-reducing Fe(II) oxidizer *Acidovorax* sp. BoFeN1–questioning the existence of enzymatic Fe(II) oxidation. Geobiology 11:180–190. https://doi.org/10.1111/gbi.12019.
44. Chakraborty A, Roden EE, Schieber J, Picardal F. 2011. Enhanced growth of *Acidovorax* sp. strain 2AN during nitrate-dependent Fe(II) oxidation in batch and continuous-flow systems. Appl Environ Microbiol 77:8548–8556. https://doi.org/10.1128/AEM.06214-11.
45. Straub KL, Schönhuber WA, Buchholz-Cleven BE, Schink B. 2004. Diversity of ferrous iron-oxidizing, nitrate-reducing bacteria and their involvement in oxygen-independent iron cycling. Geomicrobiol J 21:371–378. https://doi.org/10.1080/01490450490485854.
46. Chan CS, Fakra SC, Edwards DC, Emerson D, Banfield JF. 2009. Iron oxyhydroxide mineralization on microbial extracellular polysaccharides. Geochim Cosmochim Acta 73:3807–3818. https://doi.org/10.1016/j.gca.2009.02.036.
47. Hegler F, Posth NR, Jiang J, Kappler A. 2008. Physiology of phototrophic iron(II)-oxidizing bacteria: implications for modern and ancient environments. FEMS Microbiol Ecol 66:250–260. https://doi.org/10.1111/j.1574-6941.2008.00592.x.
48. Kappler A, Newman DK. 2004. Formation of Fe(III)-minerals by Fe(II)-oxidizing photoautotrophic bacteria. Geochim Cosmochim Acta 68:1217–1226. https://doi.org/10.1016/j.gca.2003.09.006.
49. Klueglein N, Zeitvogel F, Stierhof Y-D, Floetenmeyer M, Konhauser KO, Kappler A, Obst M. 2014. Potential role of nitrite for abiotic Fe(II) oxidation and cell encrustation during nitrate reduction by denitrifying bacteria. Appl Environ Microbiol 80:1051–1061. https://doi.org/10.1128/AEM.03277-13.
50. Wu W, Swanner ED, Hao L, Zeitvogel F, Obst M, Pan Y, Kappler A. 2014. Characterization of the physiology and cell–mineral interactions of the marine anoxygenic phototrophic Fe(II) oxidizer *Rhodovulum iodosum*–implications for Precambrian Fe(II) oxidation. FEMS Microbiol Ecol 88:503–515. https://doi.org/10.1111/1574-6941.12315.
51. Chan CS, Fakra SC, Emerson D, Fleming EJ, Edwards KJ. 2011. Lithotrophic iron-oxidizing bacteria produce organic stalks to control mineral growth: implications for biosignature formation. ISME J 5:717–727. https://doi.org/10.1038/ismej.2010.173.
52. Chan CS, De Stasio G, Welch SA, Girasole M, Frazer BH, Nesterova MV, Fakra S, Banfield JF. 2004. Microbial polysaccharides template assembly of nanocrystal fibers. Science 303:1656–1658. https://doi.org/10.1126/science.1092098.
53. Miot J, Benzerara K, Obst M, Kappler A, Hegler F, Schädler S, Bouchez C, Guyot F, Morin G. 2009. Extracellular iron biomineralization by photoautotrophic iron-oxidizing bacteria. Appl Environ Microbiol 75:5586–5591. https://doi.org/10.1128/aem.00490-09.
54. Tominski C, Lösekann-Behrens T, Ruecker A, Hagemann N, Kleindienst S, Mueller CW, Höschen C, Kögel-Knabner I, Kappler A, Behrens S, Löffler FE. 2018. Insights into carbon metabolism provided by fluorescence *in situ* hybridization-secondary ion mass spectrometry imaging of an autotrophic, nitrate-reducing, Fe(II)-oxidizing enrichment culture. Appl Environ Microbiol 84:e02166-17. https://doi.org/10.1128/AEM.02166-17.
55. Kamp A, Høgslund S, Risgaard-Petersen N, Stief P. 2015. Nitrate storage and dissimilatory nitrate reduction by eukaryotic microbes. Front Microbiol 6:1492. https://doi.org/10.3389/fmicb.2015.01492.
56. Jørgensen BB, Gallardo VA. 1999. *Thioploca* spp.: filamentous sulfur bacteria with nitrate vacuoles. FEMS Microbiol Ecol 28:301–313. https://doi.org/10.1016/S0168-6496(98)00122-6.
57. Fossing H, Gallardo VA, Jørgensen BB, Hüttel M, Nielsen LP, Schulz H, Canfield DE, Forster S, Glud RN, Gundersen JK, Küver J, Ramsing NB, Teske A, Thamdrup B, Ulloa O. 1995. Concentration and transport of nitrate by the mat-forming sulphur bacterium *Thioploca*. Nature 374:713–715. https://doi.org/10.1038/374713a0.
58. Kelly DP, Postgate JR, Kelly DP. 1982. Biochemistry of the chemolithotrophic oxidation of inorganic sulphur. Philos Trans R Soc Lond B Biol Sci 298:499–528. https://doi.org/10.1098/rstb.1982.0094.
59. Nelson DC, Jørgensen BB, Revsbech NP. 1986. Growth pattern and yield of a chemoautotrophic *Beggiatoa* sp. in oxygen-sulfide microgradients. Appl Environ Microbiol 52:225–233. https://doi.org/10.1128/aem.52.2.225-233.1986.
60. Timmer-ten Hoor A. 1981. Cell yield and bioenergetics of *Thiomicrospira denitrificans* compared with Thiobacillus denitrificans. Antonie Van Leeuwenhoek 47:231–243. https://doi.org/10.1007/BF00403394.
61. Jørgensen BB, Nelson DC. 2004. Sulfide oxidation in marine sediments: geochemistry meets microbiology. Geol Soc Am Spec Pap 379:63–81. https://doi.org/10.1130/0-8137-2379-5.63.
62. Ehrenreich A, Widdel F. 1994. Anaerobic oxidation of ferrous iron by purple bacteria, a new type of phototrophic metabolism. Appl Environ Microbiol 60:4517–4526. https://doi.org/10.1128/aem.60.12.4517-4526.1994.
63. Widdel F, Bak F. 1992. Gram-negative mesophilic sulfate-reducing bacteria, p 3352–3378. *In* Balows A, Trueper HG, Dworkin M, Harder W, Schleifer KH (ed), The prokaryotes. Springer, New York, NY.
64. Schaedler F, Lockwood C, Lueder U, Glombitza C, Schmidt C. 2017. Microbially mediated coupling of Fe and N cycles by nitrate-reducing Fe(II)-oxidizing bacteria in littoral freshwater sediments. Appl Environ Microbiol 84:e02013-17. https://doi.org/10.1128/AEM.02013-17.
65. Muyzer G, de Waal EC, Uitterlinden AG. 1993. Profiling of complex microbial populations by denaturing gradient gel electrophoresis analysis of polymerase chain reaction-amplified genes coding for 16S rRNA. Appl Environ Microbiol 59:695–700. https://doi.org/10.1128/aem.59.3.695-700.1993.
66. Zeitvogel F, Burkhardt CJ, Schroeppel B, Schmid G, Ingino P, Obst M. 2017. Comparison of preparation methods of bacterial cell-mineral aggregates for SEM imaging and analysis using the model system of *Acidovorax* sp. BoFeN1. Geomicrobiol J 34:317–327. https://doi.org/10.1080/01490451.2016.1189467.
67. Störiko A, Pagel H, Mellage A, Cirpka OA. 2021. Does it pay off to explicitly link functional gene expression to denitrification rates in reaction models? Front Microbiol 12:684146. https://doi.org/10.3389/fmicb.2021.684146.
68. Coleman TF, Li Y. 1996. An interior trust region approach for nonlinear minimization subject to bounds. SIAM J Optim 6:418–445. https://doi.org/10.1137/0806023.